Resolving the Enhanced Flow Parameters for an In-depth Analysis of the MRI- Neuroimaging

Conference Paper · April 2014

CITATIONS
2

READS
18

Resolving the Enhanced Flow Parameters for an In-depth Analysis of the MRI- Neuroimaging

M.E Emetere[1,*], O.B Awojoyogbe[2], U.E Uno[2], K.U Isah[2] and O.M Dada[2]

[1]Department of Physics, Covenant University, Canaan land, P.M.B 1023, Ota-Nigeria

(moses.emetere@covenantuniversity.edu.ng)

[2]Department of Physics, Federal University of Technology, P.M.B 1023, Minna-Nigeria

(awojoyogbe@yahoo.com , uno_essang@yahoo.co.uk)

Abstract. The functionality of current neuroimaging using the MRI machine needs to be improved to diagnose more complex problems. A new mathematical concept based on the solutions of the Bloch NMR for MRI applications was adopted to resolve functionality problems- by the inclusion of molecular interactions. The signal loss factor 'E' caused by fluctuating velocity due to compartmental boundaries in the macromolecular sites was proposed to be the vital factor required for clinical diagnosis of cognitive impairment.

Keywords: Bloch NMR,MRI, Neuroimaging, Cognitive impairment

1 Introduction

Magnetic Resonance Imaging (MRI) is a preferred tool for clinical imaging because of its advantages which includes: the absence of ionizing radiation increased imaging flexibility, and better tissue contrast. The safety in the use of MRI is commendable though it is still associated with patient claustrophobia, and the presence of metal implants [1, 2]. Aside the common application of MRI in brain imaging, it measures the brain volume, especially medial temporal lobe structures; it study the population of common brain disease e.g. Alzheimer's disease [3,4] e.t.c. Recently, a group of scientist discovered the possibility of diagnosing cognitive impairment using MRI via imaging sequence. Therefore, the multiplication of knowledge by scientists, engineers, mathematicians and clinicians on the MRI is boundless.

The use of fundamental mathematical concepts based on the solutions of Bloch NMR equation for MRI is definitely a novel idea [5,6,7,8,9,10] though there are still unanswered questions on the extent of its applicability. The Bloch NMR equations are basically about magnetizations of flowing spins

under given radio-frequency excitations and are dependent on the flow velocity of spins for measuring blood flow rate – velocity and volume flow rates. However, the non-inclusion of molecular markers which defines the pathology of macromolecular interactions in the original Bloch theorem restricts its research coverage. Therefore the need of a modified Bloch NMR is paramount for future clinical investigations of biological systems.
In this paper, we shall include the mathematical molecular marker into the ab-initio Bloch NMR equations and apply the results using different image and pulse sequencing to the MRI -neuroimaging.

2 Methods

2.1 Resolution of the Bloch NMR/MRI for Biological Systems

The inclusion of the molecular dynamic to the Bloch NMR for adequate application to clinical diagnosis shall be the focus in this section. The molecular dynamics includes the macromolecular interaction which can be evidently seen in the variation of relaxation times between tissues due to compartmental boundaries and other molecular obstacles.
In order to account for the molecular dynamics of the Bloch approach in a continuous wave nuclear magnetic resonance (CW NMR) flow equation, we propose a generic Hamiltonian to incorporate both the Bloch NMR and Molecular dynamics

$$H_T = H_{Bloch} + H_{Molecular} \tag{1}$$

H_{Bloch} is represented by the flow magnetization equation derived by Awojoyogbe et al.,[6,8-9]

$$H_{Bloch} = v^2 \frac{\partial^2 M_y}{\partial x^2} + v\left(\frac{1}{T_1} + \frac{1}{T_2}\right)\frac{\partial M_y}{\partial x} + \left(\frac{1}{T_1 T_2} + \gamma^2 {B_1}^2\right) M_y - \frac{\gamma B_1 M_o}{T_1} \tag{2}$$

$$H_{Molecular} = \frac{\partial E}{\partial x_i}\frac{\partial E}{\partial x_j} \tag{3}$$

All parameters maintain its original interpretations. Along the i^{th} site, the elastic model for macromolecular interactions is predominant therefore, $E = \sum_i^N V(x_i) + \sum_{i=2}^N \frac{1}{2} k(x_i - x_{i-1})^2$, Along j^{th} site the energy E coincide with the energy levels worked out by Emetere [11] for NMR studies. $V(x_i)$ is the potential across compartmental boundaries. This factor is important for analyzing both microscopic and macroscopic imaging techniques.

$$E = 1 - m\,.\,\omega_1 M_y \mathrm{T}_1 \tag{4}$$

Where $\omega_1 = -\gamma B_1$ the Rabi frequency, μ is the magnetic moment, M_y is the applied transverse magnetization and T_1 is the spin –lattice relaxation time.

Assume $m\,.\,\omega_1 M_y \mathrm{T}_1 \gg 1$, equation (3) can be further spitted into equation(5&6). This method is usually done in the matrix form

$$\frac{\partial E}{\partial x_j} = \mu.\,\omega_1 \mathrm{T}_1 \frac{\partial M_y}{\partial x} \tag{5}$$

$$\frac{\partial E}{\partial x_i} = \sum_i^N \frac{\partial V(x_i)}{\partial x} + \sum_{i=2}^N \frac{1}{2} k(x_i - x_{i-1})^2 \tag{6}$$

Therefore, the total Hamiltonian can be written as

$$H_T = v^2 \frac{\partial^2 M_y}{\partial x^2} + v\left(\frac{1}{T_1} + \frac{1}{T_2} + \mu.\,\omega_1 \mathrm{T}_1\right)\frac{\partial M_y}{\partial x} + \sum_i^N \frac{\partial V(x_i)}{\partial x} + \left(\frac{1}{T_1 T_2} + \gamma^2 {B_1}^2\right) M_y - \frac{\gamma B_1 M_o}{T_1} \tag{7}$$

We assume $\sum_{i=2}^N \frac{1}{2} k(x_i - x_{i-1})^2 = 0$ for the gray-white matter of the brain. Applying the Schrödinger i.e. $H\psi = E\psi$, equation [7] transforms into

$$v^2 M_y \frac{\partial^2 \psi}{\partial x^2} + \left[v\left(\frac{1}{T_1} + \frac{1}{T_2} + \mu.\,\omega_1 \mathrm{T}_1\right) M_y + \sum_i^N V(x_i)\right]\frac{\partial \psi}{\partial x} + \left[\left(\frac{1}{T_1 T_2} + \gamma^2 {B_1}^2\right) M_y - E - \frac{\gamma B_1 M_o}{T_1}\right]\psi = 0 \tag{8}$$

ψ had been calculated by Emetere [11] for NMR studies. It is summarized as $\psi = A exp(i\omega t)$. In order to analyze the time-independent domain, we place $t = \frac{xr}{\omega}$, where x is the circumference of the base sector of the cone, r is the radial component. Therefore,

$$\psi = A exp(ixr) \tag{9}$$

Substituting equation (9) into equation (8) yields two sets of governing equations

$$v^2 r^2 M_y + \left(\frac{1}{T_1 T_2} + \gamma^2 {B_1}^2\right) M_y - E - \frac{\gamma B_1 M_o}{T_1} = 0 \tag{10}$$

$$v\left(\frac{1}{T_1} + \frac{1}{T_2} + \mu.\,\omega_1 \mathrm{T}_1\right) M_y + \sum_i^N V(x_i) = 0 \tag{11}$$

The governing equations yields the following solutions

$$M_y = \frac{E T_1 T_2 + \gamma B_1 M_o T_2}{v^2 r^2 T_1 T_2 + 1 + \gamma^2 {B_1}^2 T_1 T_2)} \tag{12}$$

$$M_y = \frac{T_1 T_2 \sum_i^N V(x_i)}{(\tau + \mu.\omega_1 {T_1}^2 T_2) v} \tag{13}$$

Where $\tau = T_1 + T_2$. If $v^2 r^2 T_1 T_2 \ll 1$ and $E T_1 T_2 \ll 1$, the equation (12) yields,

$$M_y = \frac{\gamma B_1 T_2 M_o}{1 + \gamma^2 {B_1}^2 T_1 T_2} \tag{14}$$

Equation (14) is the exact solution of the CW NMR and is expressed in the laboratory frame as

$$M_{xo} = \frac{-\sin(\omega t)\gamma B_1 T_2 M_o}{1 + \gamma^2 {B_1}^2 T_1 T_2} \tag{15}$$

$$M_{yo} = \frac{\cos(\omega t)\gamma B_1 T_2 M_o}{1 + \gamma^2 {B_1}^2 T_1 T_2} \tag{16}$$

This result had been reported by numerous researchers [5], [10] i.e. showing the validity of our approach. Also, if $\mu.\omega_1 {T_1}^2 T_2 \gg \tau$, equation (13) yields a new exact solution of the CW NMR i.e.

$$M_y = \frac{\sum_i^N V(x_i)}{\mu.\omega_1 T_1 v} \tag{17}$$

The exact solution of CW NMR in a laboratory frame can also be written as

$$M_{xo} = \frac{-\sin(\omega t)\sum_i^N V(x_i)}{\mu.\omega_1 T_1 v} \tag{18}$$

$$M_{yo} = \frac{\cos(\omega t)\sum_i^N V(x_i)}{\mu.\omega_1 T_1 v} \tag{19}$$

Therefore, the flow velocity of the spin can be calculated in its raw form as

$$v = \frac{\left(1+\gamma^2 {B_1}^2 T_1 T_2\right)\sum_i^N V(x_i)}{\mu.\omega_1 \gamma B_1 M_o T_1 T_2} \tag{20}$$

if $\gamma^2 {B_1}^2 T_1 T_2 \gg 1$,

$$v = \frac{\gamma B_1 \sum_i^N V(x_i)}{\mu.\omega_1 M_o} \tag{21}$$

Therefore the flow velocity of the spin in the laboratory frame can be written as

$$v_{xo} = \frac{-\sin(\omega t)\gamma B_1 \sum_i^N V(x_i)}{\mu.\omega_1 M_o} \tag{22}$$

$$v_{yo} = \frac{\cos(\omega t)\gamma B_1 \sum_i^N V(x_i)}{\mu.\omega_1 M_o} \tag{23}$$

3. **Results**

In practical application for tissue, the T_1 is in the range of 3 to 80ms [12-13], the selective and nonselective pulse is in the range 40MHz to 200MHz [14], E in equation (12) is the energy required to optimize signal-to-noise ratios to enhance better final images [15]. The field strength required is within the range 1.5T to 4.0T [16] though voxels of grayish-white matter are usually of lesser field strength say 1.5T to 2.0T.

In order to compute the sections of the brain, we assume four sections with its peculiar compartmental boundaries as shown in the figure (1) below i.e. skull, blood, water and grayish-white matter. We proposed varying potentials V(x) for the four sections with respect to their physical properties i.e. solid, liquid and aqueous. Blood and water are liquids with different viscosity; their values were proposed as shown in equation (22). From the trend of the general flow parameters, it is scientific to assume that the potential across liquid takes the partial quadratic form as shown below. The potential across the skull was assumed to be unity though experimentally, it varies in individual because of bone density. The gray-white tissues (which includes cortical grey matter,

subcortical white matter e.t.c.) of the brain were assumed to possess an exponential potential due to its macromolecular interactions.

$$V(x) = \begin{cases} x_s : x \\ x_b : x^2 + x \\ x_w : \frac{x^2}{16} + \frac{x}{4} \\ x_g : \exp(xr) \end{cases}$$

(22)

In this model, $V(x_i)$ is the theoretical slice selection technique that defines the arterial spin
labeling timing, arterial transit delay and the apparent decay time of the signal. Depending on the part of the body, $V(x_i)$ could be modeled using polynomial expansion schemes e.g Boubaker, Chebyshev, Legendre, Bessel e.t.c. In this study, we adopted equation (22) to magnify the abnormal signals associated to diverse process errors during neuroimaging.

Fig. 1. Neuroimaging of the brain (Retrieved on 2/11/13, http://health.shorehealth.org/imagepages/19224.htm)

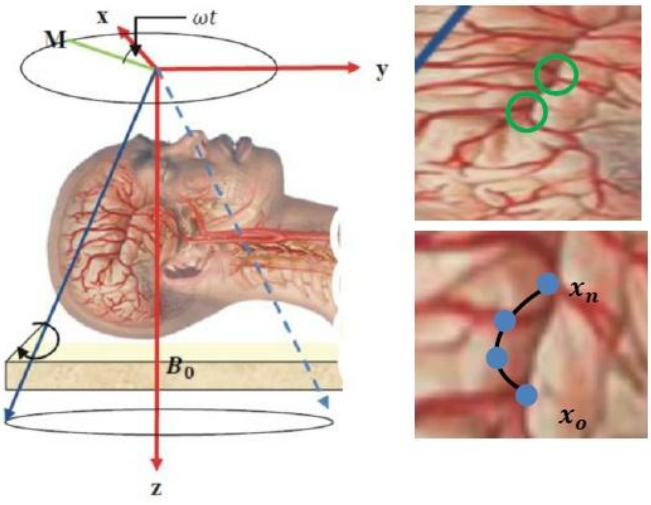

The spin velocity for different neurological examination is shown in the figure (2) below. The doted green line signifies an abnormal Headache in patients, the dotted black line signifies an abnormal neurological examination and the red dotted line signifies the existence of neurological symptoms. The spin velocity at each case is affected by the abnormal expansion of the blood vessels in the brain i.e. endothelium. Therefore, a sudden increase in measured speed signifies the presence of neurological symptoms.

Fig. 2. signaling interpretation of Experimental Data

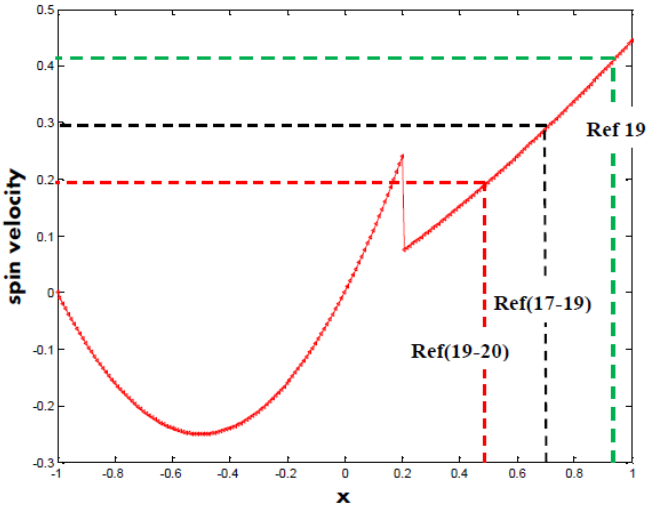

Fig. 3. signaling in a Myo laboratory frame

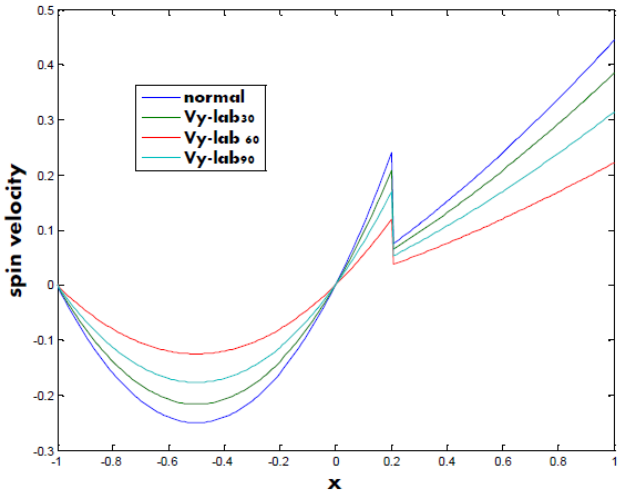

The effects of the nominal tip angle of various rf excitations on the spin flow was investigated (using $\frac{\pi}{2}, \frac{\pi}{3}, \frac{\pi}{6}$)as shown in figure (3-5). At this point the transverse magnetization is believed to be constant.

The first rf excitation occurs when the nominal tip angle is $\pi/3$. This idea is quite different from the sequence suggested in ref (21). The positive (figure 4) and negative (figure 5) velocity in a laboratory frame was also investigated. While the negative spin velocity follows the normal rf pulse pattern, the posi-

tive spin velocity opens up the reality of signal loss in the Bloch flow systems e.g. stenotic flow [22].

Fig. 4. signalling in a Mxo laboratory frame

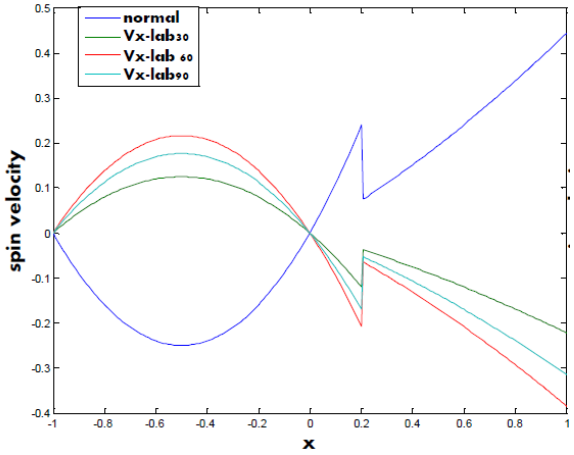

Fig. 5. signalling in a recoiled Mxo laboratory

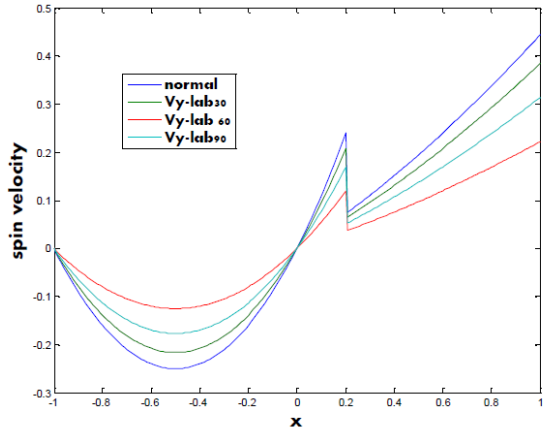

One of the objectives of this paper is to resolve the signal loss which is majorly caused by fluctuating velocity. As can be seen in figure (6), when the spin velocity flows across the x-axis of the brain, its transmission through the compartmental boundaries of the gray-white matter of the brain experiences an internal deviation which increase the size of the spin packet from $\gamma B_1 M_o$ to $(E + \gamma B_1 M_o)$. This event produces blurred images which are corrected by the use of digital signal processors. In reality, the additional factor 'E' ought not to be screened away but harvested in order to measure more complex problem

like cognitive impairment. For example, we propose that the farther deviated a scattered signal from its originating packet (or higher value of 'E'), the greater the cognitive impairment.

Fig. 6. signaling abnormities in neuroimaging

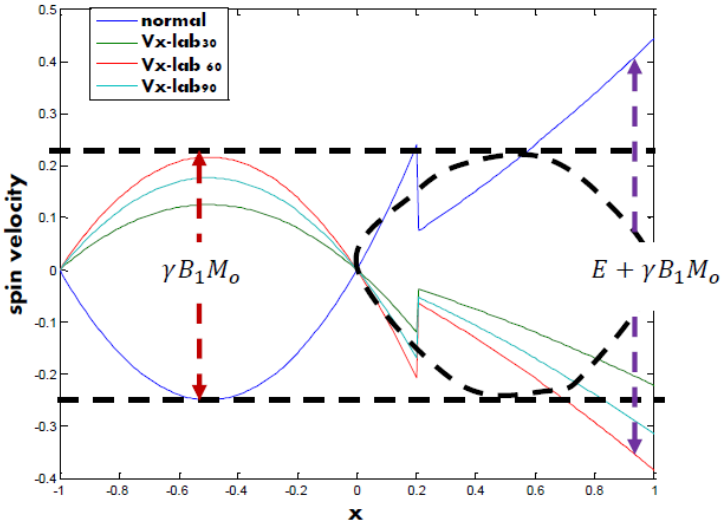

4 Conclusions

The additive functionality to the Bloch NMR flow equations has been improved upon - the possibilities in the MRI-neuroimaging to detect with accuracy more complex problems in neurological examination. The signal loss due to fluctuating velocity as it transmits through compartmental molecular boundaries is also essential for higher diagnostic selection to determine the degree of cognitive impairment in patient. The introduction of the potential across segregated states of matter within the living tissue is a leeway for introducing higher mathematical techniques into the solutions of Bloch NMR equation for MRI applications.

Appreciation.

The authors appreciate the contributions of both institutions.

Reference.

1. George, A.E., de Leon, M.J., Stylopoulos, L.A., Miller, J., Kluger, A., Smith, G.:. CT diagnostic features of Alzheimer disease: Importance of the

choroidal/hippocampal fissure complex. Am J Neuroradiol 11, 101–107(1990)
2. Jobst, K.A., Smith, A.D., Szatmari, M., Molyneux, A., Esiri, M.E., King, E.: Detection in life of confirmed Alzheimer's disease using a simple measurement of medial temporal lobe atrophy by computed tomography. Lancet.340, 1179–1183(1992).
3. Varma, A.R., Snowden, J.S., Lloyd, J.J., Talbot, P.R., Mann, D.M., Neary, D.: Evaluation of the NINCDS-ADRDA criteria in the differentiation of Alzheimer's disease and frontotemporal dementia. J. Neurol Neurosurg Psychiatry 66, 184–188 (1999).
4. Linn, R.T., Wolf, P.A., Bachman, D.L., Knoefel, J.E., Cobb, J.L., Belanger, A.J., The 'preclinical phase' of probable Alzheimer's disease. A 13-year prospective study of the Framingham cohort. Arch Neurol. 52, 485–490 (1995).
5. Odoh, E. O. and De, D. K.: Application of Nuclear Magnetic Resonance Imaging in Blood Flow Estimation. The African Physical Review 3, 65-74 (2009).
6. Awojoyogbe, O. B., Dada, M., Faromika, O. P., Moses,O. F., Fuwape, I. A.: Polynomial Solutions of Bloch NMR Flow Equations For Classical and Quantum Mechanical Analysis of Fluid Flow in Porous Media. Open Magnetic Resonance Journal 2, 46 (2009).
7. Jain,V., Langham, M. C., Wehrli, F. W.: MRI estimation of global brain oxygen consumption rate. J. of Cerebral Blood Flow &Metabolism 30, 1598 (2010).
8. Awojoyogbe,O. B., Faromika, O. P., Dada, M.,Ojambati, O. S., Boubaker, K. Mathematical Models of real Geometrical Factors in Restricted Blood vessels for the Analysis of CAD (Coronary Artery Diseases) Using Legendre, Boubaker and Bessel polynomials J.Med. Syst. 9, 9428 (2010).
9. Awojoyogbe, O. B., Dada, M., Faromika,O. P., Dada, O. E.: Mathematical Concept of the Bloch Flow Equations for General Magnetic Resonance Imaging. Concepts in Magnetic Resonance Part A 38A, 85 (2011).
10. De, D. K.: NMR/MRI Blood Flow Magnetization Equation in the Rotating Frame of Reference: Part I. The African Physical Review 8, 201 (2013).
11. Emetere, M.E.: Mathematical Modeling of Bloch NMR to Solve the Schrodinger Time Dependent Equation. The African Review of Physics 8, 65-68 (2013).

12. Bloom, M., Holmes, K.T., Mountford, C.E.,Williams,P.G.:Complete proton magnetic resonance in whole cells. Magn. Reson. 69, 73-91 (1986).
13. Peemoeller, H., Shenoy, R.K., Pintar, M.M., Kydon, D.W., Inch, W.R.: Improved Characterization of Healthy and Malignant Tissue by NMR Line-Shape Relaxation Correlations. Biophys. Journal 38, 271- 295 (1982).
14. Sobol,W.T., Cameron, I.G., Inch, W.R., Pintar,M.M.: Modeling of proton spin relaxation in muscle tissue using nuclear magnetic resonance spin grouping and exchange analysis. Biophys. Journal. 50, 181-191 (1986).
15. Lee, J .N., Riederer,S.J.: The contrast-to-noise in relaxation time, synthetic, and weighted-sum MR images. Magn. Reson. Med. 5, 13-22 (1987).
16. Jezzard, P., Balaban R.S.: Correction Of Geometric Distortion In Echo-Planar Images Bo Field Variations. Magn. Reson. Med. 34, 65-73(1995)
17. Duarte, J., Sempere, A.P., Delgado, J.A., Naranjo, G., Sevillano, M.D., Claveria, L.E.: Headache of recent onset in adults: a prospective population-based study. Acta Neurol Scand. 94, 67-70 (1996).
18. Larson, E.B., Omenn, G.S., Lewis, H.: Diagnostic evaluation of headache. Impact of computerized tomography and cost-effectiveness. JAMA. 243, 359-362 (1980).
19. Mitchell, C.S., Osborn, R.E., Grosskreutz, S.R.: Computed tomography in the headache patient: is routine evaluation really necessary? Headache 33, 82-86 (1993).
20. Kahn Jr , C.E., Sanders, G.D., Lyons, E.A., Kostelic, J.K., MacEwan, D.W., Gordon,W.L.: Computed tomography for nontraumatic headache: current utilization and cost-effectiveness. Can Assoc Radiol J. 44, 189-193(1993).
21. Wladyslaw, T. S.: Medical Applications of NMR. Bulletin of Magnetic Resonance11, 69-85(1989)
22. Siegel Jr, J., Oshinski, J., Pettigrew, R., Ku, D.: Computational simulation of turbulent signal loss in 2D time-of-flight magnetic resonance angiograms. Magnetic Resonance in Medicine 37, 609-614 (19